A Comparative Study of Energy-efficient Driving Strategy for Connected Internal Combustion Engine and Electric Vehicles at Signalized Intersections

Haoxuan Dong[a, 1], Weichao Zhuang[a, 1], Boli Chen[b], Yan Wang [a], Yanbo Lu [a], Ying Liu [a], Liwei Xu [a], Guodong Yin[a,*]

[a] School of Mechanical Engineering, Southeast University, Nanjing 211189, China

[b] Department of Electronic and Electrical Engineering, University College London, London, UK

[*] Corresponding author, E-mail address: ygd@seu.edu.cn; Tel.: +86-13913879060

[1] These authors contributed equally to this work

HIGHLIGHTS

- An eco-driving control strategy is proposed for vehicles approaching a signalized intersection.
- The discharge of the vehicle queue is modeled and predicted.
- The proposed strategy is based on a computationally efficient iterative dynamic programming algorithm.
- Monte-Carlo simulation using real-world traffic data is performed for in-depth energy efficiency analysis.
- Energy-saving potential enabled by the proposed strategy is investigated for both internal combustion engine and electric vehicles.

Abstract: This paper takes into consideration of vehicle queues at the intersection and proposes an energy-efficient driving strategy to improve vehicle energy efficiency and overall traffic throughput in an urban traffic environment. The proposed strategy is applicable for both electric vehicle and internal combustion engine vehicle, and the control framework is formed by three sections, a vehicle queue discharge predictor, a spatial-domain optimal control strategy for energy consumption minimization, and a speed tracker with consideration of collision avoidance constraints. The former is based on the intelligent driver model, which predicts an accurate vehicle queue discharge time. Then the iterative dynamic programming is utilized to find the optimal solutions with fast computational speed. Finally, the optimal speed profile is followed by a Proportion-Integration controller while keeping a safe inter-vehicular distance. A Monte-Carlo simulation is designed to evaluate the energy efficiency of the proposed strategy in the stochastic traffic environment. Compared to the regular eco-approach and departure and constant speed strategies that lack awareness of the queue, significant energy saving can be achieved of the proposed strategy. In addition, three typical cases are selected to study the energy efficiency when the proposed strategy is applied to internal combustion engine and electric vehicles, respectively. The results show the energy efficiency of electric vehicles is less sensitive to the queuing effect at the intersection because of regenerative braking and the overall higher efficiency of the electric motor in contrast to the internal combustion engine, especially in stop-and-go scenarios.

Keywords: eco-driving control, connected vehicle, speed optimization, traffic prediction, iterative dynamic programming

1. Introduction

Traffic lights are developed for safe traffic management [1]; however, inefficient operation of the traffic signal could aggravate traffic congestion [2], and therefore increases vehicle fuel consumption and emissions [3, 4]. A variety of methods have been proposed from two fundamental perspectives to improve traffic throughput and vehicle energy efficiency at a signalized intersection. The first one is to optimize traffic light signal phase and timing (SPaT) for prioritization of vehicles approaching the intersection, such as the traffic light priority control for emergency vehicles [5], buses [6], and trucks [7]; the cooperative optimization of traffic signal and vehicle, for efficient driving control of a single vehicle [8] or a platoon [9].

On top of that, vehicle dynamics can be controlled to reduce the overall energy consumption required to complete the mission. Available methods include powertrain control [10], regenerative braking control [11], and eco-driving control [12].

Among them, the eco-driving control that targets an energy-efficient speed profile is recognized as one of the most effective methods [13, 14] to improve vehicle energy efficiency and traffic throughput [15, 16], and therefore have great potential for commercialization in the near future [17].

The eco-driving control at a signalized intersection is also called eco-approach and departure (EAD) control [18]. Recent advancements of vehicular connectivity technologies enable vehicles to access the SPaT information in real-time so that predictive eco-driving strategies were developed for enhanced energy efficiency and traffic throughput at a signalized intersection [19]. Katsaros *et al*. [20] developed a speed advisory system to minimize fuel consumption and stop delays subject to the given SPaT information. The goal of this algorithm is to reduce idling time at a red signal. Mahler *et al*. [21] introduced a stochastic signal phase prediction model that is integrated into the velocity optimization scheme to maximize the chance of going through an intersection at a green light. Han *et al*. [22] proposed a platoon-based trajectory optimization method, to reduce fuel consumption of multiple vehicles passing through a signalized intersection. Another study presented by Lin *et al*. [23] solved the energy-efficient speed in presence of multiple signalized intersections by an energy-aware driving strategy. More recently, Mousa *et al.* [24] presented a deep reinforcement learning agent for solving the EAD problem in the vicinity of signalized intersections for minimization of fuel consumption, which does not require prior knowledge of vehicle and traffic environment.

Most studies mentioned above assume the vehicle driving under free-flow traffic. In real world traffic conditions, the vehicle speed may be restricted by the preceding vehicle or the queue waiting at an intersection [25]. In such conditions, regular EAD strategies may fail to deliver energy-efficient driving profiles or may even lead to a rear-end collision due to the unexpected traffic ahead. To enhance the eco-driving strategy in real traffic situations, Xie *et al.* [26] used radar to detect the movement of the preceding vehicle and developed an eco-driving strategy for intersection crossing. Zeng *et al.* [27] investigated speed optimization subject to a given route with multiple signalized intersections. However, the speed profiles of the lead vehicles are known as a priori, which is impractical. He *et al.* [28] optimized the vehicle trajectory considering the queue at a signalized intersection relying on ideal Vehicle-to-Vehicle and Vehicle-to-Infrastructure (V2I) technologies. In the real world, the vehicle may encounter mixed driving scenarios. To this end, Guo *et al*. [29] presented a hybrid reinforcement learning based eco-driving algorithm considering both the speed and the lane changing operations, for simultaneous fuel economy and travel time optimization by using historical driving data. Wang *et al*. [30] proposed a hierarchical eco-driving strategy for adapting mixed driving scenarios. This strategy relies on the information of traffic light SPaT obtained by the V2I communication and the preceding vehicle detected by the millimeter wave radar. However, such full connectivity capabilities cannot be realized overnight [31]. This has motivated research on EAD strategies with partial and possibly disrupted vehicular connectivity. Shao *et al*. [32] proposed a predictive EAD strategy, where the movement of the preceding traffic is predicted by using Unscented Kalman Filter in conjunction with a simple traffic flow model. Sun *et al*. [33] designed a data-driven eco-driving control approach by considering various uncertainties associated with traffic signal SPaT. Bakibillah *et al*. [34] developed a stochastic eco-driving strategy. The influences of both uncertain behaviors of preceding vehicles and duration of signal phases are indirectly modeled by the probabilistic crossing time for finding the energy-optimal speed. Another EAD is proposed by Yang *et al.* in [35], where the strategy ensures the arrival of the vehicle at the intersection stop line immediately after the last queued vehicle is discharged to ensure minimal waiting time at the intersection.

Existing research work mainly focuses on the internal combustion engine vehicle (ICEV). The electrification of the automotive industry poses new research opportunities about eco-driving of an electric vehicle (EV) [36], since the EV and ICEV have different eco-driving strategies due to their different powertrain systems and energy consumption models [37, 38, 39]. One of the major differences between the EV and ICEV is that an EV can recover kinetic energy by using regenerative braking, which usually leads to a different energy-optimal speed profile [40, 41]. In [42], Han *et al*. solved the eco-driving problems for both EV and ICEV by using analytic optimization methods to find the fundamental properties of the driving profile in both cases. However, the work was based on highly

simplified vehicle and energy consumption models that neglect aerodynamic drag and powertrain losses. The resulting solution could be considerably different from reality. Gao *et al*. [43] also investigated the eco-driving behavior for the EV and ICEV. Although the explicit powertrain models are included, the study was based on a non-optimal control strategy, which cannot reflect the optimal driving behavior.

This paper proposes an energy-efficient driving strategy (EEDS) that is compatible with both EV and ICEV, followed by a thorough comparative investigation of their energy-saving potential with the control mechanism at a signalized intersection, where vehicle queues play a key role in eco-driving control. The main contributions of this paper are threefold:

1) The movement of the vehicle queue is predicted by using the intelligent driver model (IDM), which involves both vehicle dynamics and driver behavior.
2) A new eco-driving strategy with the awareness of the preceding queuing vehicles is proposed to identify the optimal speed profile approaching a signalized intersection. The proposed strategy integrates the IDM-based queue predictor and a speed optimizer based on the iterative dynamic programming (IDP), which can rapidly find the optimal solution.
3) A Monte-Carlo simulation case study is investigated to verify the energy efficiency improvement in different driving conditions for both EV and ICEV. The results provide significant insight into the energy-saving potential over eco-driving and the effect of vehicle queue on the energy efficiency of both vehicle types.

The remainder of this paper is organized as follows. Section 2 provides the vehicle dynamics and energy consumption models, followed by the mathematical formulation of the eco-driving control problem. The proposed EEDS strategy is presented in Section 3. In Section 4, stochastic simulations and numerical comparisons are conducted to show the effectiveness of the EEDS. Section 5 discusses the energy efficiency for EV and ICEV when applying the proposed EEDS strategy. Finally, concluding remarks are given in Section 6.

2. Problem formulation

This section formulates vehicle dynamics and the eco-driving problem at a traffic intersection.

2.1 Vehicle dynamics

2.1.1 Longitudinal dynamics

In this paper, the following vehicle longitudinal dynamics are considered [44]

$$m\delta\dot{v}(t) = F_v(t) - F_r(t) \tag{1}$$

where m is the vehicle mass, δ is the vehicle rotational inertia coefficient, $v(t)$ is the vehicle speed, $F_v(t)$ is the traction force, and $F_r(t)$ is the resistance force. As the work focuses on daily driving, where vehicle accelerations are remarkably smaller than adherence limits, it is reasonable to assume that the wheels do not slip at their contact point with the ground but can rotate freely about their axes of rotation [45]. Thus, during driving, the traction force is determined by the powertrain torque $T_p(t)$

$$F_v(t) = T_p(t)i_g(t)i_0\eta_t r_w \tag{2}$$

where $i_g(t)$ is the transmission ratio, fixed for an EV and variable for an ICEV. i_0 is the final drive ratio, r_w is the radius of vehicle tires, and η_t is the driveline efficiency. During braking, the negative vehicle force involves mechanical brakes for an ICEV and both regenerative and mechanical braking forces for an EV. Besides, F_r is composed of aerodynamic drag, rolling resistance, and gravity force, as shown in Eq. (3),

$$F_r(t) = mgf\cos\theta + mg\sin\theta + 0.5C_D A\rho v(t)^2 \tag{3}$$

where g is the acceleration of gravity, f is the rolling resistance coefficient, C_D is the aerodynamic drag coefficient, A is the frontal area, ρ is the air density, and θ is the road slope.

2.1.2 Energy consumption model

This part introduces the energy consumption models of both EV and ICEV. For an EV that is powered by a centralized electric motor (EM), a quasi-static model [46] is built up to calculate the battery power by Eq. (4)

$$P_b(t) = P_m(t)\eta_m^{-\mathrm{sign}(P_m(t))}\eta_b^{-\mathrm{sign}(P_m(t))} \tag{4}$$

where $P_b(t)$ is battery power, positive for discharging and negative for charging. $P_m(t)$ is the EM power. Similar to the battery power, we use the convention that when it works as a motor, power as well as the load torque are positive, and the power is assumed negative when it works as a generator. $\mathrm{sign}()$ is a signum function. η_b is battery efficiency, which is assumed to be constant in this paper. η_m is the EM efficiency, which is determined by its speed and torque as shown in Fig. 1.

For ICEV, the powertrain is composed of an internal combustion engine (ICE) that drives the wheels via a continuously variable transmission (CVT), which is proved to be more efficient when driving in an urban area due to its ability to continuously change its gear ratio [47]. As with the EM, the ICE is also modeled by the steady-state modeling approach [48]. As such, the engine fuel consumption rate $\dot{m}_f$ is a function of the engine speed $\omega_e(t)$ and engine torque $T_p(t)$, expressed as

$$\dot{m}_f(t) = \Psi\left(\omega_e(t), T_p(t)\right) P_e(t) \tag{5}$$

where $P_e(t)$ is the ICE output power, $\Psi()$ represents the brake-specific fuel consumption (BSFC) map, as shown in Fig. 2, and the idling speed for the ICE is 600 rpm. The ICEV also includes an engine start-stop system (SSS) that enables the ICE to be switched off to reduce idling losses. In this paper, it is assumed that the SSS control consistently switches off the engine (ω_e =0 rpm and $\dot{m}_f = 0$) when the vehicle stops ($v = 0$).

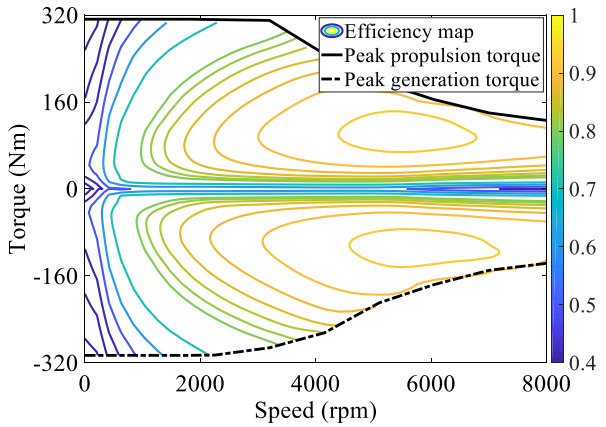

Fig. 1. The efficiency map and peak torque of the EM.

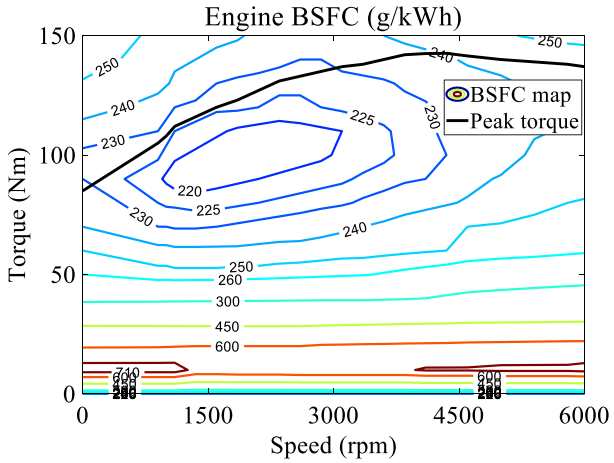

Fig. 2. The BSFC map and peak torque of the ICE.

2.2 Optimal control problem

Fig. 3 shows the schematic of the problem addressed in this paper. As it can be seen, vehicles are limited to single-lane driving so that lane-changing and overtaking are not allowed for the ego vehicle. Moreover, when the ego vehicle enters the communication/control zone, the traffic light is red and all the preceding vehicles approaching the intersection are stationary (i.e., the queue for the traffic light is at a complete standstill). The traffic signal transition time from red to green is denoted by T_s. It is also assumed that all vehicles can traverse the intersection within a green interval that lasts T_{gr} seconds.

The ego vehicle is equipped with a V2I device (Dedicated Short-Range Communication or LTE-V) and therefore traffic information at the intersection is enabled by communicating with the Road Side Unit (RSU) at the traffic light. The length of the communication/control zone is D, which is determined by the communication range of the RSU. The target of eco-driving in this work is to minimize the energy consumption and travel time of the ego vehicle required to cross the stop line subject to collision avoidance constraints.

Now, we can formulate the problem as an optimal control problem (OCP) [25], that follows:

$$\underset{\boldsymbol{u}}{\text{minimize}} \quad J\big(u(t), x(t)\big) = \int_0^{t_p} E\big(u(t), x(t)\big)dt \tag{6}$$

s.t.

$$\dot{x}(t) = f(x, u, t) \tag{7a}$$

$$\phi(x, u, t) \leq 0 \tag{7b}$$

$$\beta\left(x(0), x\left(t_p\right)\right) = 0 \tag{7c}$$

where $E\big(u(t), x(t)\big)$ represents the electric power for the EV and the fuel consumption rate for the ICEV, t_p is the moment when the ego vehicle crosses the stop line at the intersection, which is influenced by the vehicle queue discharge time and SPaT. $u(t)$ is the control input. For the EV case, $u(t) = F_v(t)$ with $F_v(t)$ the driving force act on the wheels. For the ICEV case, $u(t) = [F_v(t) \quad i_g(t)]^{\mathrm{T}}$ with the additional state i_g for the gear ratio of the CVT. $x(t) = [d(t) \quad v(t)]^{\mathrm{T}}$ is the vehicle state vector, formed by vehicle travel distance $d(t)$ and speed $v(t)$.

Furthermore, the differential constraint Eq. (7a) collects Eq. (1) and

$$\dot{d}(t) = v(t) \tag{8}$$

with the boundary conditions $d(0) = 0, v(0) = v_s, d\left(t_p\right) = D, v\left(t_p\right) = v_{des}$ that are taken into account by Eq. (7c). Note

that v_s is predefined initial speed, whereas v_{des} is determined by the stop line crossing speed of the last vehicle in the queue. Eq. (7b) represents the state and input constraints for the problem. First, to avoid rear-end collision, the ego vehicle needs to keep a safe inter-vehicular distance d_{safe} with the lead vehicle that is the last one in the queue

$$[D - d(t)] - d_q(t) \geq d_{safe}(t) \tag{9}$$

where $d_q(t)$ is the distance from the rear end of the last vehicle in the queue to the stop line. To improve traffic throughput and to prevent the vehicle from violating the road speed limit, the vehicle minimum and maximum speeds are limited by Eq. (10)

$$v_{min} \leq v(t) \leq v_{max} \tag{10}$$

The vehicle traction force follows Eq. (11), which limits the maximum acceleration and deceleration of the vehicle to ensure driving comfort.

$$F_{vmin} \leq F_v(t) \leq F_{vmax} \tag{11}$$

where $F_{vmin} < 0$ is the maximum braking force and $F_{vmax} \geq 0$ is the maximum propulsion force. Finally, for the ICEV case, the CVT gear ratio is constrained by Eq. (12)

$$i_{g,min} \leq i_g(t) \leq i_{g,max} \tag{12}$$

It is worth noting that v_{des}, d_q, and t_p of the OCP are unknown and are influenced by the discharge of the queuing vehicles. In the next section, we propose a synthetic eco-driving control strategy to address the OCP Eqs. (6) and (7) in presence of those unknowns.

3. Energy-efficient driving strategy

The control strategy that addresses the OCP (Eqs. (6) and (7)) formulated in Section 2 is introduced in this Section. The framework of EEDS is depicted in Fig. 3. It is formed by three major schemes: the vehicle queue discharge predictor, the

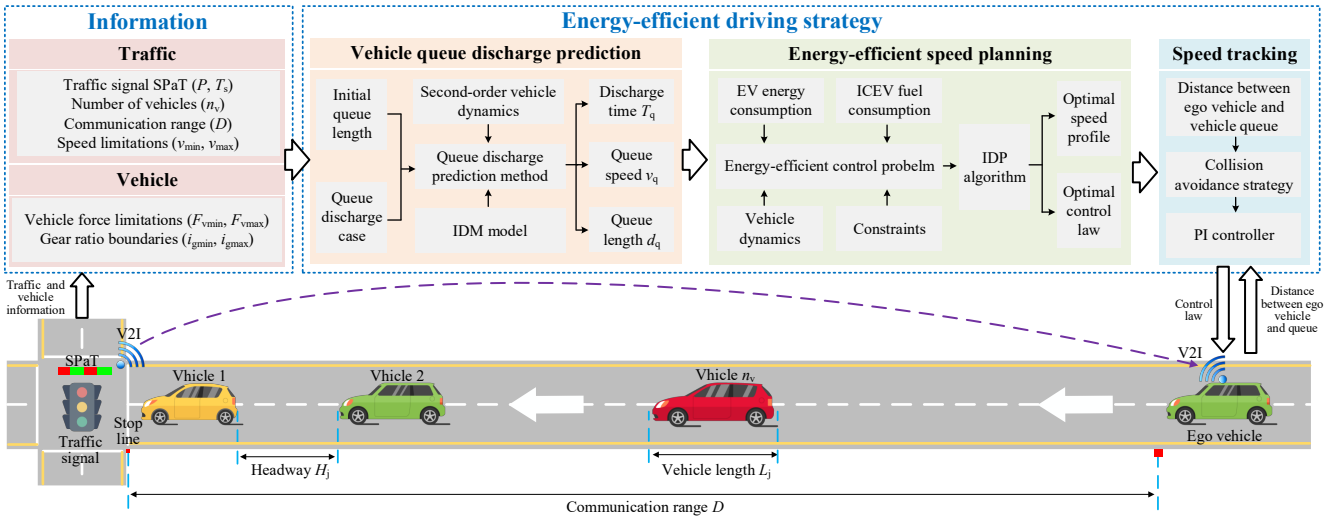

Fig. 3. The schematic of vehicles traveling towards a signalized intersection and the control framework of the proposed EEDS.

energy-efficient speed planner, and the speed tracker for safety purposes. The former predicts the queue discharge time and speed of the last vehicle, and then the information is used by an IDP-based speed optimizer to find the most energy-efficient speed profile for the ego vehicle. However, the optimal velocity trajectory found by IDP cannot guarantee a safe separation distance between the ego and the vehicle in front due to the unavoidable prediction error. To this end, a collision avoidance strategy is deployed in conjunction with a Proportion-integration (PI) controller to follow the IDP solution in a safe manner.

3.1 Vehicle queue discharge prediction

In this study, it is assumed that the ego vehicle accesses the SPaT information and the number of vehicles n_v in the queue from the RSU. The n_v is acquired by using widely used in-ground loop detectors [49]. Let us index vehicles in the queue from 1 to n_v starting from the vehicle closest to the stop line. The distance from the rear end of the jth vehicle to the stop line is defined as $d_j(0)$ and calculated by Eq. (13)

$$d_j(0) = \sum_{1}^{j} (L_j + H_j) \tag{13}$$

where L_j is the body length of the jth vehicle, H_j is the standstill spacing between the *j*th vehicle and it preceding one, and H_1 represents the space between the first vehicle and the stop line. Thus, the queue length $d_q(0)$ is equal to the distance of the n_vth vehicle to the stop line, that is $d_q(0) = d_{n_v}(0)$.

Let v_j and a_j are the velocity and acceleration of *j*th vehicle in the queue, respectively, the movement of queuing vehicles can be predicted by

$$\begin{cases} v_j(t) = 0 & t < T_j \\ \dot{v}_j(t) = a_j(t) & t \geq T_j \end{cases} \tag{14}$$

where T_j is the time instant when the *j*th vehicle starts moving when the traffic light changes to the green signal. Considering κ_j the reaction time of the driver of the *j*th vehicle. It is immediate to obtain $T_j = T_s + \sum_1^j \kappa_j$.

To predict the acceleration of each vehicle, we employ the IDM, which is a well-accepted model for single-lane traffic flow [50]. From the IDM, the acceleration of the *j*th vehicle follows

$$a_j(t) = a_{max}\left(1 - \left(\frac{v_j(t)}{v^*}\right)^{\varpi} - \left(\frac{s^*(t)}{s_j(t)}\right)^2\right) \tag{15}$$

with

$$s^*(t) = s_0 + \max\left[0, T_{h,j}v_j(t) + \frac{v_j(t)\left(v_j(t) - v_{j-1}(t)\right)}{2\sqrt{a_{min}a_{max}}}\right]$$

where $a_{min} < 0$ and $a_{max} \geq 0$ are respectively the maximum deceleration and acceleration of each vehicle for comfort purposes. v^* is the desired velocity, which equals the predefined maximum allowed speed. $s_j(t)$ is the spacing between *j*th vehicle and the vehicle immediately ahead. $s^*(t)$ is the desired gap between two consecutive vehicles, s_0 is the acceptable minimum following distance, ϖ is the acceleration exponent, and $T_{h,j}$ is the safety time headway of the *j*th vehicle.

With the velocity prediction of queuing vehicles, the instantaneous queue length $d_q(t)$ can be estimated by

$$d_q(t) = d_q(0) - \int v_{n_v}(t)dt \tag{16}$$

and the discharging time of queue, T_q is defined as

$$d_q(T_q) = 0 \tag{17}$$

For clarity, the implementation algorithm for the vehicle queue discharge prediction is given in Algorithm 1.

Algorithm 1 Implementation algorithm for the vehicle queue discharge prediction

Input: n_v , L_j, H_j, κ_j, and T_s
Output: T_q and v_{des}
1. Initial by setting $t = 0$, $j = 1$, and sampling time Δt_q = 0.01s
2. $d_q(0) \leftarrow \sum_{j=1}^{j=n_v}(L_j + H_j)$
3. **while** $d_{n_v}(t) \leq d_q(0)$
4. **for** $j \leftarrow 1{:}\,1{:}\,n_v$
5. **if** $t = 0$
6. $v_j(t) \leftarrow 0$
7. $d_j(t) \leftarrow d_j(0)$
8. **else**
9. **if** $t \leq T_s + \sum_1^j \kappa_j$
10. $v_j(t) \leftarrow 0$
11. $d_j(t) \leftarrow d_j(0)$
12. **else**
13. $v_j(t) \leftarrow v_j(t - \Delta t_q) + \Delta t_q a_j(t)$
14. $d_j(t) \leftarrow d_j(t - \Delta t_q) - 0.5\Delta t_q\left(v_j(t - \Delta t_q) + v_j(t)\right)$
15. **end if**
16. **end if**
17. **end for**
18. $t \leftarrow t + \Delta t_q$
19. **end while**
20. Set $T_q \leftarrow t$, $v_{des} \leftarrow v_{n_v}(t)$

3.2 Iterative dynamic programming

3.2.1 Fundamentals of dynamic programming

This section introduces the IDP-based speed planner. In contrast to the DP, the IDP can significantly reduce the computation burden by adaptively refining the search space at each iteration.

Since the traveled distance of the ego vehicle to pass through the stop line is fixed at D (that is determined by the communication range of the RSU) whereas the travel time is uncertain, it is reasonable to reformulate the time-domain OCP (see Eqs. (6) and (7)) into the space-domain, as expressed in Eq. (18), with N the total number of distance steps. Consider Δd the sampling interval of the distance, it holds that $N = D/\Delta d + 1$.

$$\begin{aligned} \underset{\boldsymbol{u}}{\text{minimize}}\ J\big(u(k), x(k)\big) = \sum_{k=1}^{N} E\big(u(k), x(k)\big)\, t(k) \\ +\alpha_1(v(N) - v_{des})^2 + \alpha_2\big(t(N) - T_q\big)^2 \end{aligned} \tag{18}$$

s.t.

$$\begin{gathered} u_{min} \leq u(k) \leq u_{max} \\ v_{min} \leq v(k) \leq v_{max} \\ T_q \leq t(N) = t_p \leq T_s + T_{gr} \\ v(k+1) = \sqrt{v^2(k) + 2a(k)\Delta d} \\ a(k) = \frac{F_v(k) - F_r(k)}{m\delta} \end{gathered}$$

where $x(k)$ is the state vector, i.e., $x(k) = [v(k), t(k)]$, and $u(k)$ is the control variable, i.e., $u(k) = F_v(k)$ for the EV and $u(k) = \left[F_v(k), i_g(k)\right]$ for the ICEV. $t(k)$ is the required time to travel from $(k-1)$th distance step to the next and it can be approximated by Eq. (19)

$$t(k) = \frac{\Delta d}{0.5(v(k) + v(k-1))} \tag{19}$$

For ease of computation, the terminal distance and velocity conditions in Eq. (7) are converted to soft constraints in Eq. (18) as the latter two terms, which can drive the states to the desired terminals. It is noteworthy that the terminal time is limited (third constraint in Eq. (18)) so that the ego vehicle can pass through the stop line before the traffic signal switches back to red. In addition, α_1 and α_2 are weighing factors for two terminal costs.

The OCP in Eq. (18) can be solved recursively by following the Bellman Principle [51] and the steps for the basic DP are shown in Fig. 4.

3.2.2 Iterative dynamic programming algorithm

Although DP can derive the global optimal solution, the high computational cost limits its applicability. For this reason, in this study we use the IDP, which deploys the DP iteratively with rescaled state and control constraints and grids to moderate computational burden [52]. The relationship between the IDP and DP is shown in Fig. 4. As it can be seen, coarse grids are employed in the first instance, and the density of the grid points and the feasibility region of state and control change gradually to recursively achieve the problem solving.

The rescaling mechanism of the grids is illustrated in Fig.5. The IDP is initialized with coarse grids (Δx_1 and Δu_1 for the initial state and control) and the initial search region that is defined by the state and control constraints. Without loss of generality, let us assume that it yields the optimal control rule $u_{opt,1}$ and state profile $x_{opt,1}$. Then, the bounds of control inputs and states at the (i+1)th iteration ($x_{min,i+1}$, $x_{max,i+1}$) and ($u_{min,i+1}$, $u_{max,i+1}$) are redefined based on the solution found in the previous iteration,

$$\begin{aligned} x_{max,i+1} &= \min\left(x_{optU,i} + \tau\Delta x_i, x_{max}\right) \\ x_{min,i+1} &= \max\left(x_{optL,i} - \tau\Delta x_i, x_{min}\right) \end{aligned} \tag{20}$$

$$\begin{aligned} u_{max,i+1} &= \min\left(u_{optU,i} + \sigma\Delta u_i, u_{max}\right) \\ u_{min,i+1} &= \max\left(u_{optL,i} - \sigma\Delta u_i, u_{min}\right) \end{aligned} \tag{21}$$

where $x_{optU,i}$, $x_{optL,i}$, $u_{optU,i}$ and $u_{optL,i}$ are the maximum and minimum values of state and control variables at the ith iteration, respectively. $\tau \le 1$ and $\sigma \le 1$ are the scaling coefficients for constraints of state and control variables. Δx_i and Δu_i are the grid sizes for the ith iteration, which are defined by reduction factors $\gamma < 1$ and $\lambda < 1$.

$$\Delta x_{i+1} = \gamma \Delta x_i \tag{22}$$

$$\Delta u_{i+1} = \lambda \Delta u_i \tag{23}$$

Consider the maximum allowed iterations I_{max}. The IDP algorithm terminates when the conditions are satisfied.

$$E_{opt,i} \le \vartheta E_{opt,i-1} \text{ or } i > I_{max} \tag{24}$$

where ϑ is the user-defined parameter for the compromise between accuracy and convergence speed. In other words, the IDP keeps rescaling and solving the resulting OCP unless the solution converges or it the maximum number of iterations is reached. It should be noted that the parameters τ, σ, γ, λ, and ϑ could affect the calculation speed and optimization accuracy.

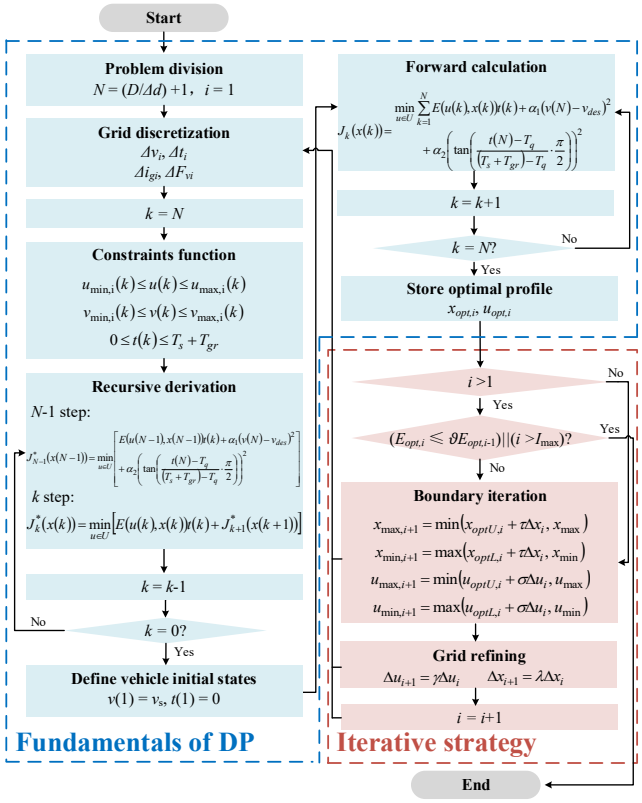

Fig. 4. The flowchart of the IDP algorithm. Here the blue modules represent the DP algorithm, and the red modules represent the iterative strategy.

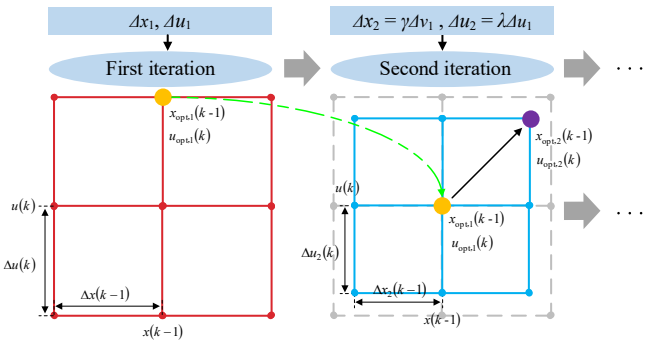

Fig. 5. The grid rescaling diagram of the IDP algorithm.

3.3 Collision avoidance velocity tracking strategy

In this study, a PI-based speed tracker is designed for speed tracking with consideration of the collision avoidance strategy. In the PI controller, the speed error is used as the input, and the acceleration is defined as the output to achieve precise tracking of the target speed. Let v_d be the optimal velocity trajectory of IDP. Following v_d derived from the IDP may result in rear-end collision due to the inevitable prediction error. Thus, a collision avoidance strategy [53] is adopted to ensure a safe following distance between the ego vehicle and the last vehicle in the queue. The strategy is described by

$$v(k+1) = \begin{cases} v_d(k) & \text{if } H_v(k) > d_c(k) \\ v(k) + a_{min}\Delta t & \text{if } d_s(k) < H_v(k) \le d_c(k) \\ v(k) + a_\varphi \Delta t & \text{if } H_v(k) \le d_s(k) \end{cases} \tag{25}$$

with

$$d_c(k) = H_0 + \left(v(k) - v_{n_v}^*(k)\right)\Delta t + \frac{v^2(k) - v_{n_v}^{*2}(k)}{2|a_{min}|}$$

$$d_s(k) = H_0 + \left(v(k) - v_{n_v}^*(k)\right)\Delta t + \frac{v^2(k) - v_{n_v}^{*2}(k)}{2|a_\varphi|}$$

where d_c is the minimum distance for driving comfort, d_s is the minimum distance for driving safety, H_0 is a "static gap" and determines the minimum gap when the vehicle stops. Δt is the sampling time in the simulation. $a_\varphi < 0$ is the deceleration limited by road adhesion, $v_{n_v}^*$is the actual velocity of the last vehicle in the queue, H_v is the bumper-to-bumper inter-vehicle distance of the ego vehicle and the n_vth vehicle in the queue. It should be noted that the safety distance is generally shorter than the detectable distance of the vehicle radar, thus the rear-end collision avoidance control is enabled when the preceding vehicle is detected.

4. Simulation results and discussion

To evaluate the performance of the proposed EEDS strategy, this section conducts a series of simulations in MATLAB and SUMO environments. The PC for simulation has an Intel Core i7-8700 @ 3.20GHz processor and 16G RAM.

4.1 Simulation setup

All simulation examples are carried by considering an EV and an ICEV, respectively, and the results obtained in both scenarios are compared. The vehicle model characteristics (e.g., mass, air drag coefficients, front area) are taken from the C-Class hatchback 2012 vehicle in CarSim (version 20959, 2016.1). For the EV, the battery, electric motor, and final drive are chosen according to the existing equipment in our laboratory. For the ICEV, the engine, transmission, and final drive are sized from the experimental data in ADVISOR such that the EV and ICEV have similar driving performances, e.g., maximum acceleration and maximum speed. The ego vehicle parameters in both scenarios are summarized in Table 1. The traffic system is modeled in SUMO, and the queue is formed by using SUMO's car-following model. We simulate the traffic environment by using real-world traffic, i.e., the intersection of Shuanglong Avenue and Yanhu Road, Nanjing, China. Table 2 shows the associated traffic parameters used in the case study [54, 55].

Table 1
Main parameters of EV and ICEV in simulation.

Component		Parameter	Value
Vehicle		Mass m	1421 kg
		Front area A	2.22 m^2
		Aerodynamic drag coefficient C_D	0.3
		Air density ρ	1.206 kg·m^{-3}
		Rotational inertia coefficient δ	1.022
		Rolling resistance coefficient f	0.015
		Wheel radius r_w	0.325 m
		Acceleration of gravity g	9.8 m·s^{-2}
EV	EM	Maximum power	103.9 kW/-98.1 kW
		Maximum torque	312.5 Nm/-306.3 Nm
	Li-ion battery	Capability	52 kWh
		Voltage	360 V
		Efficiency η_b	0.9
	Powertrain	Transmission ratio i_g	1
		Final drive ratio i_o	5.12
		Driveline efficiency η_t	0.9
ICEV	ICE	Volume	1.8 L
		Maximum Power	101.7 kW
		Maximum Torque	143.1 Nm
	Powertrain	Transmission ratio i_g	0.4~3.4
		Final drive ratio i_o	3.3
		Driveline efficiency η_t	0.9

4.2 Benchmark strategies

The proposed EEDS is compared with two existing strategies: constant speed (CS) [56] and regular EAD (READ) [57] for benchmarking purposes.

When the CS strategy is in use, the ego vehicle approaches the intersection with constant cruising speed. For fair comparisons, two versions of CS strategy are defined: CS (READ) and CS (EEDS), which follow the average speed of READ and EEDS, respectively. On the other hand, the READ strategy uses the a priori knowledge of SPaT information to determine the optimal speed profile [57]. Similar to the EEDS, the speed profiles that are derived from CS and READ may not be valid (lead to a rear-end collision) due to the lack of consideration of the queuing vehicles. Therefore, we adopt the same speed tracking controller introduced in Section 3.3 to generate safe counterparts of the CS and original READ solutions. To show the impact of the queuing vehicles on the optimal eco-driving behavior, we define the original solution of READ (without considering queue) as READ (original). While the safety-guaranteed solution is defined as READ.

Table 2
Main parameters of the traffic system in simulation.

Parameter	Value
Communication range D	360 m
Initial speed v_s	54 km/h
Green signal interval T_{gr}	45 s
Signal cycle length T_c	85 s
Minimum speed v_{min}	20 km/h
Maximum speed v_{max}	60 km/h
Vehicles in queue n_v	[1, 20]
Transition time T_s	[1 s, 40 s]
Standstill spacing H_j	[1 m, 3 m]
Vehicle body length L_j	[3.5 m, 5.5 m]
Maximum acceleration a_{max}	[2 m·s^{-2}, 4 m·s^{-2}]
Maximum deceleration a_{min}	[-2 m·s^{-2}, -4 m·s^{-2}]

4.3 Energy efficiency improvement in different driving conditions

To evaluate the performance of the proposed EEDS in a stochastic traffic environment, a Monte-Carlo simulation is conducted. The investigation involves 1,000 individual simulation trials for both EV and ICEV with constant D, v_s, T_c, v_{min}, and v_{max}. Traffic parameters T_s,n_v and the individual vehicle parameters H_j, L_j, a_{min}, and a_{max} are all randomized in the simulation for a thorough investigation. All the parameters are given in Table 2.

The parameters of the proposed IDP are determined first by the systematical analysis. The initial grid size of velocity is 10 km/h, the grid interval of time is 5 s, the grid size of vehicle force is 200 N, and the transmission ratio grid size is 0.5. The scaling coefficients are τ = 0.4, σ = 0.3, γ = 0.02, and λ = 0.1. The allowance coefficient ϑ is set as 0.95, that is, the iteration terminates when the step improvement of IDP is less than 5%. The maximum number of iterations I_{max} is 10. The fast computational ability of IDP is reported in the Supplementary Material.

Fig. 6 shows the box figures for energy consumption reduction of EEDS compared to READ, where the x-axis represents the number of vehicles in the queue. It should be noted that different strategies may result in different final driving speed when a vehicle approaches the stop line. Thus, to make a fair comparison, the total energy consumption of each strategy includes the consumed energy and the differences between initial and terminal kinematic energy.

As shown in Fig. 6, the EEDS achieves significant energy efficiency improvement compared to READ for both EV (16.04 % on average) and ICEV (24.25 % on average). The results indicate that the energy consumption reduction is mainly influenced by T_s and n_v. More specifically, when a few vehicles waiting at the intersection, both READ and EEDS can drive the ego vehicle to pass through the stop line without stops. As n_v grows the ego vehicle with READ was blocked by the queue due to the lack of queue discharge prediction. If n_v further increases, the velocity of the ego vehicle is highly influenced by the lengthy queue, and the benefit of using EEDS decreases. In some cases when both n_v and T_s are sufficiently large, the ego vehicle has to stop regardless of the EEDS strategy being used.

When the n_v is fixed, the energy consumption reduction is dispersedly distributed concerning T_s. This is because 1) a fast transition from red to the green signal not block the traffic at the intersection even the problem is initialized with a long queue, thus energy efficiency of EEDS with little or no improvement compared with READ; 2) the vehicle with READ was blocked by the preceding vehicles as the T_s increases, and consequently, the energy consumption increases.

Based on the results of the Monte-Carlo simulation, all traffic situations can be divided into three cases depending on the impact of the queuing vehicles on the ego vehicle (specified by n_v and T_s), 1) free-driving (no impact), 2)

saturated speed (moderate impact), and 3) with inevitable stops (significant impact). Next, further simulation was carried out to show the distance and speed trajectories of each control strategy in the three cases so that the energy efficiency improvement of the EEDS can be further shown. In Figs. 7-10, the traveled distance and speed profiles of the EEDS are benchmarked against CS and READ under the three cases, and the resulting energy consumption is reported in Tables 3 and 4.

4.3.1 Case A (free-driving)

This sub-section considers a case with n_v = 3, T_s = 7 s. Since only a few vehicles are involved in the queue and the red signal waiting time T_s is short, this scenario is less challenging compared to the remaining two.

As it can be seen in Figs. 7-10 (a), the vehicle queue is discharged in 14.8 s after the traffic signal turns to a green indication. Thus, the ego vehicle with all three strategies could pass through the intersection without stopping for the vehicle queue. As a consequence, the solution of READ (original) also can be followed precisely. In addition, both READ and EEDS strategies yield the same solution. Compared to the CS strategy, the READ and EEDS can reduce the energy consumption by 10.84 % and 13.16 % in the EV and ICEV cases, respectively.

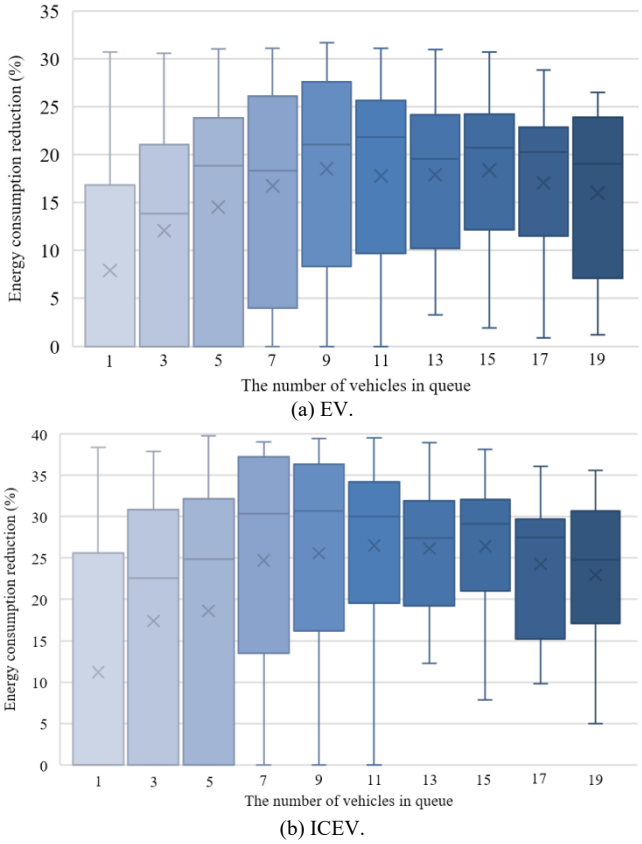

Fig. 6. Energy consumption reduction of EEDS as compared to READ in the Monte-Carlo simulation.

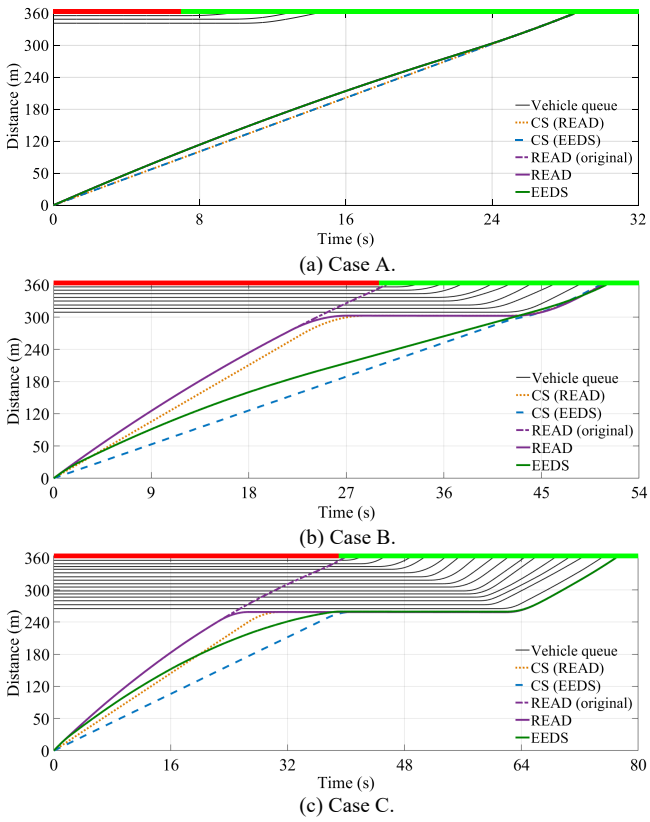

Fig. 7. Distance profiles of EEDS, REDS, and CS strategies for EV.

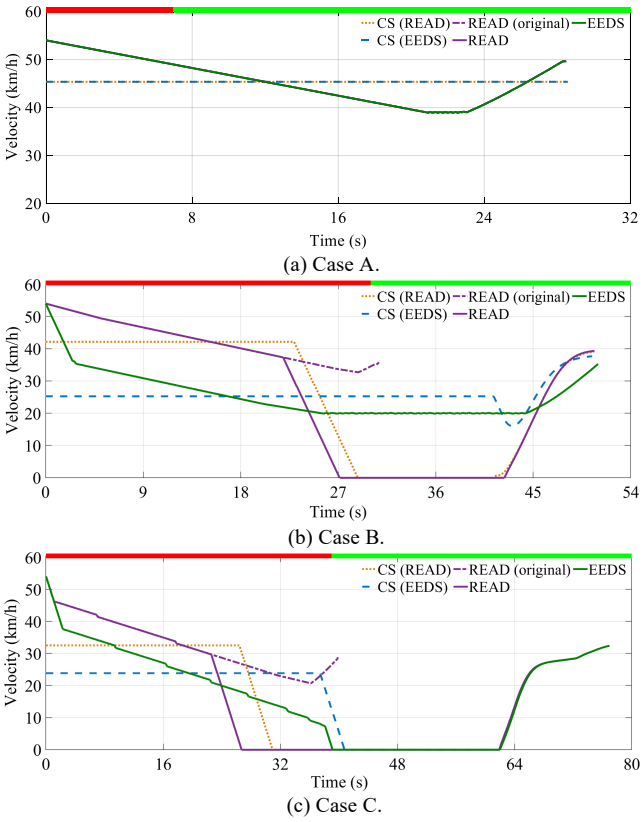

Fig. 8. Velocity profiles of EEDS, REDS, and CS strategies for EV.

Table 3
Energy consumption of EEDS, REDS, and CS strategies for EV.

	Case A			Case B			Case C		
	Battery energy	Kinetic energy changes	Improvement	Battery energy	Kinetic energy changes	Improvement	Battery energy	Kinetic energy changes	Improvement
CS (READ)	156.71 kJ	0 kJ	N/A	251.07 kJ	-13.69 kJ	N/A	221.26 kJ	-0.51 kJ	N/A
CS (EEDS)	156.71 kJ	0 kJ	N/A	233.41 kJ	43.39 kJ	N/A	234.25 kJ	26.69 kJ	N/A
READ (original)	112.80 kJ	-26.92 kJ	10.84 % (vs. CS(READ))	21.02 kJ	-93.05 kJ	56.92 % (vs. CS (READ))	17.66 kJ	-118.45 kJ	38.63 % (vs. CS(READ))
READ	112.80 kJ	-26.92 kJ	10.84 % (vs. CS(READ))	148.61 kJ	-76.30 kJ	15.05 % (vs. CS(READ))	106.77 kJ	-104.03 kJ	4.95 % (vs. CS(READ))
EEDS	112.80 kJ	-26.92 kJ	10.84 % (vs. CS(EEDS)) 0 % (vs. READ)	88.65 kJ	-93.05 kJ	4.38 % (vs. CS(EEDS)) 19.21 % (vs. READ)	103.19 kJ	-103.90 kJ	0.23 % (vs. CS(EEDS)) 1.76 % (vs. READ)

Table 4
Fuel consumption of EEDS, REDS, and CS strategies for ICEV.

	Case A			Case B			Case C		
	Fuel (Energy)	Kinetic energy changes	Improvement	Fuel (Energy)	Kinetic energy changes	Improvement	Fuel (Energy)	Kinetic energy changes	Improvement
CS (READ)	9.91 ml (330.00 kJ)	0 kJ	N/A	21.44 ml (713.95 kJ)	29.55 kJ	N/A	16.92 ml (563.44 kJ)	18.29 kJ	N/A
CS (EEDS)	9.91 ml (330.00 kJ)	0 kJ	N/A	15.47 ml (515.15 kJ)	48.15 kJ	N/A	16.93 ml (563.77 kJ)	3.74 kJ	N/A
READ (original)	7.74 ml (257.74 kJ)	-28.84 kJ	13.16 % (vs. CS(READ))	7.96 ml (265.07 kJ)	-88.81 kJ	48.29 % (vs. CS(READ))	8.05 ml (268.07 kJ)	-114.12 kJ	29.89 % (vs. CS(READ))
READ	7.74 ml (257.74 kJ)	-28.84 kJ	13.16 % (vs. CS(READ))	16.21 ml (539.79 kJ)	-74.82 kJ	10.20 % (vs. CS(READ))	19.85 ml (661.01 kJ)	-101.79 kJ	-39.92 % (vs. CS(READ))
EEDS	7.74 ml (257.74 kJ)	-28.84 kJ	13.16 % (vs. CS(EEDS)) 0 % (vs. READ)	9.16 ml (305.03 kJ)	-95.27 kJ	6.11 % (vs. CS(EEDS)) 34.87 % (vs. READ)	12.45 ml (414.59 kJ)	-101.66 kJ	16.79 % (vs. CS(EEDS)) 32.32 % (vs. READ)

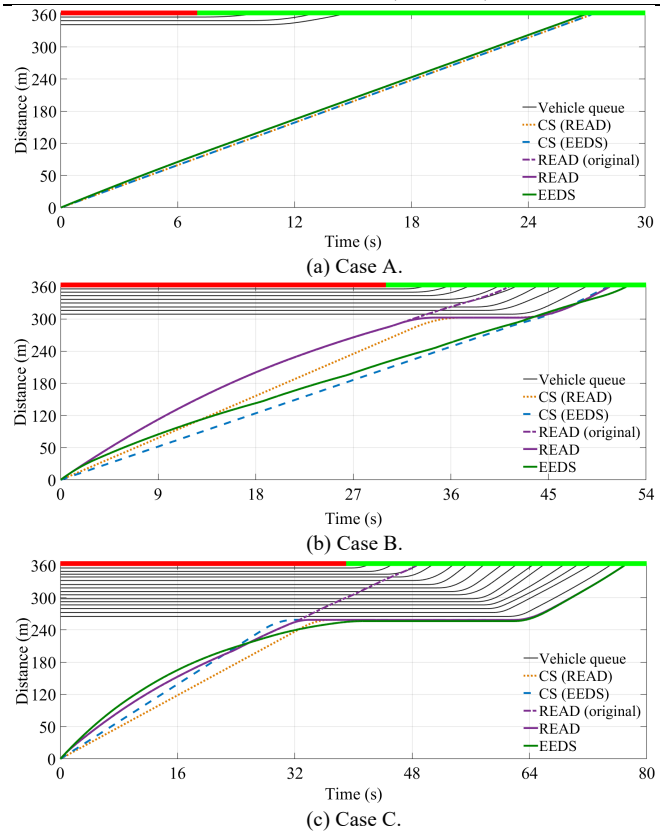

(a) Case A.
(b) Case B.
(c) Case C.

Fig. 9. Distance profiles of EEDS, REDS, and CS strategies for ICEV.

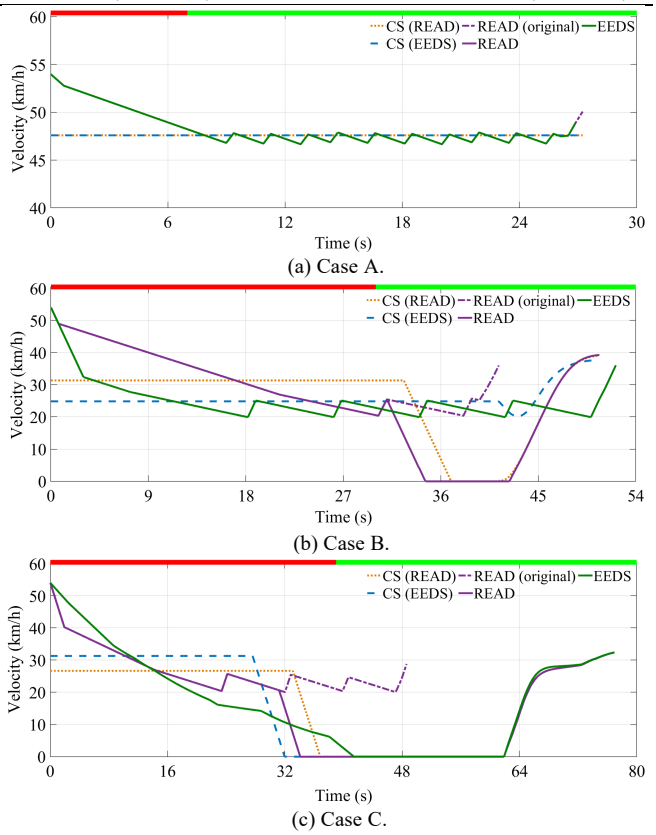

(a) Case A.
(b) Case B.
(c) Case C.

Fig. 10. Velocity profiles of EEDS, REDS, and CS strategies for ICEV.

4.3.2 Case B (saturated speed)

In this case, we let n_v = 8, T_s = 30 s. Due to the increase of both parameters, the ego vehicle has to stop if the original solutions of READ are followed.

As observed in Tables 3 and 4, compared to the CS strategy, the EEDS and READ achieve dramatic energy consumption reduction for both EV and ICEV. However, since the READ (original) does not consider the vehicle queue, the ego vehicle will be affected by the movement of the vehicle queue if the ego vehicle is following the speed profile of the original solutions of READ (see Figs. 8(b) and 10(b)). That is the presence of vehicle queue at intersection results in the partial following of the optimized speed profile of the READ (original), and more energy is consumed.

Since the EEDS considers the effects of vehicle queue, its energy efficiency is the best among all strategies for both EV and ICEV scenarios. By comparing the EV with ICEV, more energy-saving can be made when the ego vehicle is an ICEV by using the proposed EEDS. This is because the EM is more efficient than ICE in stop-and-go scenario, and the EV could recover braking energy.

4.3.3 Cas C (with inevitable stops)

By further increasing the two parameters to n_v = 15, T_s = 39s, stops are inevitable no matter following the speed profiles derived from CS, READ, or EEDS due to the long vehicle queue and traffic signal transition time.

As shown in Figs. 7(c) and 9(c), the longer red signal interval and queuing vehicles make the ego vehicle stop at the intersection for all strategies. However, the ego vehicle can still benefit from the EEDS by 0.23 % (EV) and 16.79 % (ICEV) as compared to the CS strategy. In addition, for EV and ICEV as shown in Figs. 8(c) and 10(c), only about 60 % speed profile of READ (original) is followed due to the longer vehicle queue for both EV and ICEV. Thus, the fuel consumption of READ is even higher than the CS, i.e., increased by 39.92 % as shown in Table 4.

Overall, simulation results indicate the significant influence of the vehicle queue on vehicle energy efficiency at the signalized intersection. With EEDS, both EV and the ICEV speed trajectories include three driving modes. Nevertheless, the EV follows a mode sequence decelerating/gliding down, constant speed cruising, and accelerating, whereas the ICEV follows decelerating/gliding down, repeat pulse and glide (P&G) operation, and accelerating. The P&G operation is often advised as an eco-driving mechanism of ICEV [25, 42, 57]. This is because periodically operating the ICE at a high load and then shutting it down, for a constant average vehicle speed, yields a lower fuel consumption than keeping a constant cruising speed. In addition, the energy consumption of both vehicles is completely different and varies with the traffic environment (see Tables 3 and 4). The detailed efficiency analysis of the proposed EEDS for EV and ICEV will be discussed in Section 5.

5. Efficiency analysis of the proposed EEDS for EV and ICEV

In Section 4, three typical intersection traffic cases are studied. This section investigates the energy losses of components of both EV and ICEV in order to show the energy-saving potential of the proposed EEDS and the effect of vehicle queue on energy efficiency improvement. Fig. 11 shows the energy flow of the EV and ICEV. The total energy required from the energy source (i.e., battery energy E_{bat} for the EV and fuel energy E_{fuel} for the ICEV) mainly originates from the following five elements: kinetic energy changes ΔE_{ke}, friction braking loss El_{fb}, rolling resistance loss El_{rr}, air drag loss El_{ad} and powertrain losses. The powertrain losses consist of EM, battery, and final drive losses in the EV, and ICE, transmission, and final drive for the ICEV. To sum up, the energy balance of EV and ICEV are

$$E_{bat} - \Delta E_{ke} = El_{fb} + El_{mot} + El_{bat} + El_{dl} + El_{rr} + El_{ad} \quad (26)$$

$$E_{fuel} - \Delta E_{ke} = El_{fb} + El_{eng} + El_{dl} + El_{rr} + El_{ad} \quad (27)$$

where El_{bat} is the battery internal energy loss, El_{dl} is the driveline losses, including final drive loss for the EV, and transmission loss and final drive loss for the ICEV. El_{mot} and El_{eng} are the energy losses caused by the EM and the ICE, respectively.

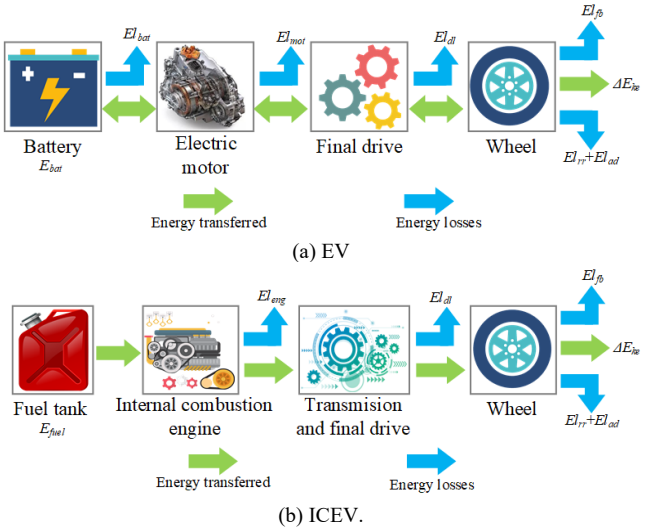

Fig. 11. The energy flow of EV and ICEV.

5.1 Energy-saving potential of proposed EEDS for EV and ICEV

Since the vehicle queue has dissipated while the ego vehicle arrives at the stop line in Case A, this case is used to represent a free flow driving scenario, and therefore it demonstrates how the proposed EEDS improve vehicle energy efficiency for EV and ICEV.

Fig. 12 shows all energy losses for both powertrain cases, and Fig. 13 displays the operating points of the EM and the ICE. As shown in Fig. 12, energy-efficient driving control does not reduce the energy loss of rolling resistance. This is mainly because they are determined by rolling coefficient, vehicle mass, and travel distance, which remain unchanged. When the vehicle speed determined by the CS (EEDS) is the average speed of EEDS, thus the El_{ad} has barely changed of EEDS compared with CS strategy. However, the EEDS could reduce the energy losses caused by the powertrain of both EV and ICEV dramatically compared to the CS strategy with the same travel time. As shown in Figs. 8(a) and 10(a), the vehicle with EEDS reaches the intersection smoothly. Thus, the associated energy losses are reduced.

Differences between the optimal driving modes of the EV and ICEV are the consequence of their different working features [25]. As shown in Fig. 13, the working points of CS strategy are fixed and located in the moderate-efficiency area. However, the EEDS tried to move the operating points of the EM and ICEV to a higher efficiency area by

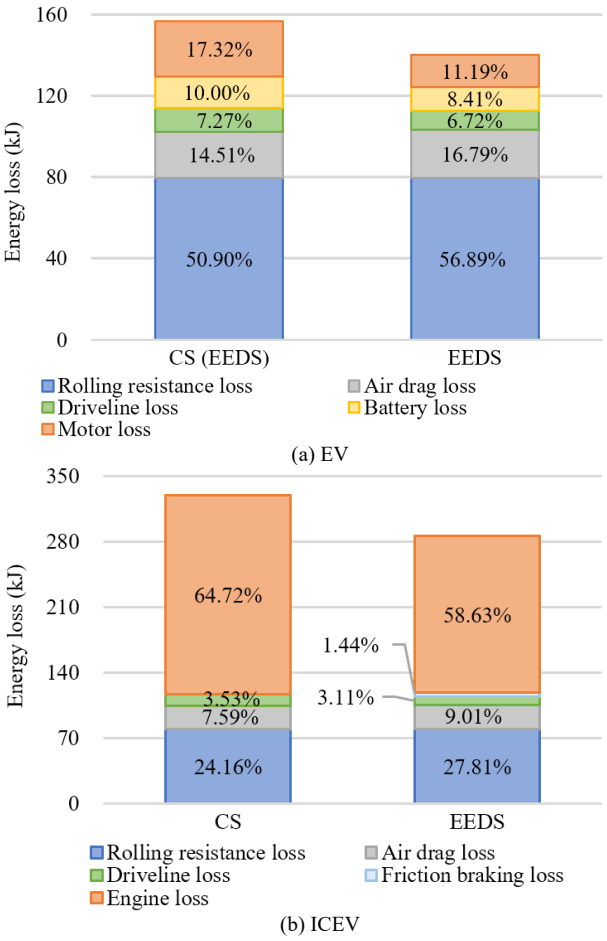

Fig. 12. Energy losses of CS and EEDS strategies in Case A.

optimizing the vehicle speeds. Specifically, the average efficiency of EM for CS and EEDS are 75.13 % and 84.32 %, respectively; the average fuel consumption rate of ICE for CS and EEDS are 0.36 ml/s and 0.25 ml/s, respectively. That is, EEDS improves vehicle energy efficiency by 10.84 % and 13.16 % for EV and ICEV, respectively.

In addition, the largest energy consumption components for the EV and ICEV are different. The majority of energy losses are caused by the ICE for the ICEV, while the EV's dominant energy loss component is rolling resistance in this case because the EV powertrain components can be operated more efficiently and the air drag loss is small due to the overall slow driving speed at an intersection.

Therefore, eco-driving could decrease energy losses via appropriate speed control. In urban traffic, ICEV can benefit more from the EEDS as compared to the EV since the electric powertrain has an overall higher efficiency, and the regenerative braking can recuperate the otherwise dissipated

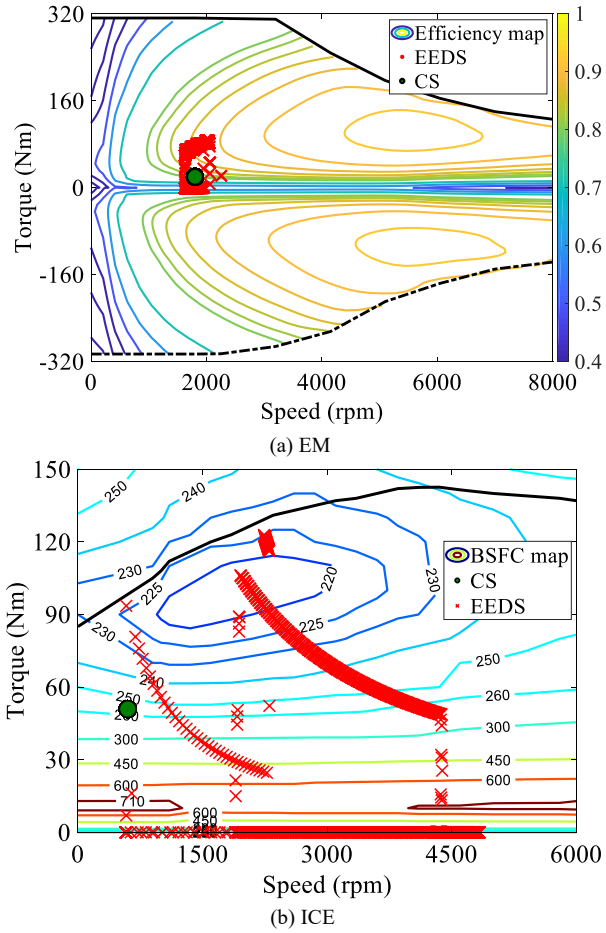

Fig. 13. Operating points of EM and ICE in Case A.

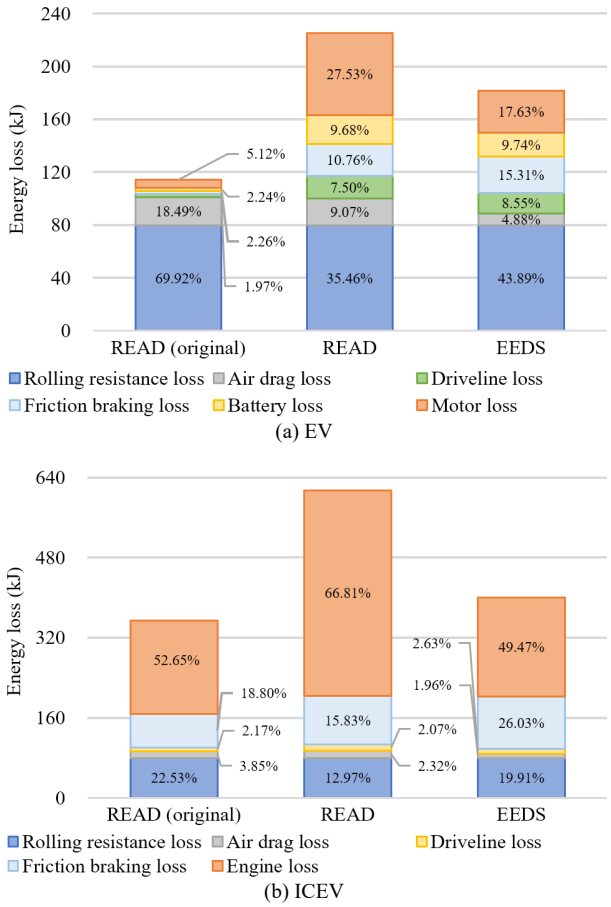

Fig. 14. Energy losses of READ and EEDS strategies in Case B.

braking energy. The effects of vehicle queues on energy consumption will be discussed in the next section.

5.2 Effect of vehicle queue on energy efficiency improvement for EV and ICEV

In Case B, the queue waiting at the intersection blocks the movement of the ego vehicle if ignoring its effect. Thus, Case B is used to demonstrate the effect of the preceding vehicle queue on energy-efficient driving for the ego EV and ICEV. The components of energy losses for the READ (original), READ, and EEDS are depicted in Fig. 14. Fig. 15 shows the and EM and ICE operating points for both EV and ICEV.

As shown in Tables 3 and 4, and Fig. 14, the READ, which does not consider queue, achieves poorer energy efficiency than EEDS. The increased energy losses of READ including El_{fb} and powertrain losses. It can be concluded from Figs. 14 and 15:

1) compared with the READ (original), the powertrain losses of READ increase significantly because ignoring the effect of queue results in lower operating efficiency of EM and ICE (see Fig. 15). The average efficiency of EM for READ (original) and READ are 83.17 % and 71.05 %, respectively; the average fuel consumption rate of ICE for READ (original) and READ are 0.19 ml/s and 0.34 ml/s, respectively. In addition, for both EV and ICEV, the powertrain losses of EEDS are higher than the READ due to the consideration of queuing vehicles. However, the EEDS achieves better energy efficiency than READ in actuality.

2) the El_{ad} for EEDS is lower than READ. Because the EEDS considers the vehicle queue predictively, it decelerates the vehicle to a lower speed since the very beginning and maintains a lower speed for most parts of the mission as shown in Figs. 8(b) and 10(b).

3) both READ and EEDS incur more friction braking loss as compared to READ (original) due to the unexpected

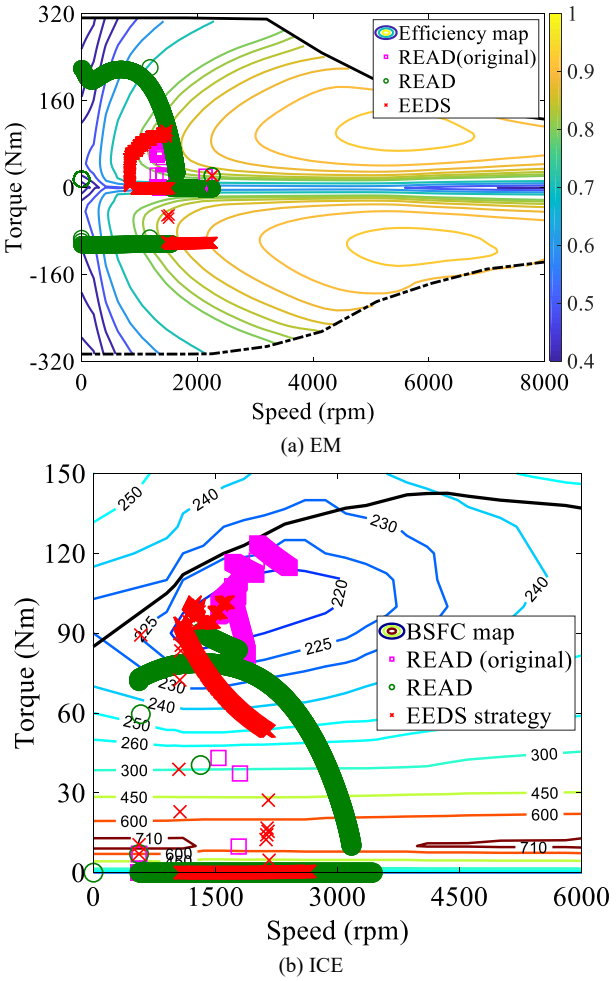

(a) EM

(b) ICE

Fig. 15. Operating points of EM and ICE in Case B.

deceleration is required to deal with the vehicle queue. In contrast to the READ, EEDS applies further braking power at the beginning (see Figs. 8(b) and 10(b)), which permits more energy-saving from the ICE, motor, and air drag losses. It should be noted that the braking energy cannot be fully recovered due to the engagement of the mechanical brake when considerable deceleration is required.

4) the most energy-consuming components in Case B are similar to Case A for both vehicles. For EEDS, there is 49.47% of energy loss is caused by the ICE for ICEV, while the most energy-consuming components in this case are similar to Case A for both EV and ICEV. For EEDS, there is 49.47% of energy loss caused by the ICE for ICEV, while only 17.63% of energy loss is from EM operation for EV. Thus, in urban traffic, the ICEVs tend to be more sensitive to stop-and-go operations caused by vehicle queues due to the characteristics of the ICE.

6. Conclusion

In this paper, an energy-efficient driving strategy is developed to minimize the energy consumption for a vehicle approaching a signalized intersection with the consideration of vehicle queue. The proposed strategy is comprised of a vehicle queue discharge predictor, an optimal speed planner, and a speed tracker. The predictor estimates the discharge time and length of the queue by using the intelligent driver model, while the optimal speed trajectory of the ego vehicle is found by the iterative dynamic programming, which can substantially reduce the computational burden of the regular dynamic programming algorithm. Finally, the optimal speed profile is followed by the Proportion-Integration controller with a specialized collision avoidance strategy.

The numerical validation of the proposed strategy involves a Monte-Carlo simulation with randomized traffic parameters so as to show the advantages of the proposed strategy against constant speed and regular eco-approach and departure strategies under different traffic environments. The results show that significant energy efficiency improvement can be achieved by using the proposed strategy as compared to the conventional eco-driving strategies for both electric vehicles and internal combustion engine vehicles, and the benefit is more significant when the ego vehicle is an internal combustion engine vehicle. Further results show that the majority of energy-saving by following the speed trajectory of the proposed strategy is from the powertrain. In the context of an internal combustion engine vehicle, the most energy-consuming component is the internal combustion engine whereas for an electric vehicle energy is mainly consumed by the rolling resistance in urban areas due to its overall higher powertrain efficiency. As a consequence, the internal combustion engine vehicle is more sensitive to stop-and-go operations caused by vehicle queue and thereby can benefit more from the eco-driving control.

Future research efforts will be devoted to developing the experimental platform for the field test of the proposed methodology to show its energy-saving potential in reality. In this context, the computational time is a major concern,

which will be further investigated and more efficient optimization formulation methods will be sought if necessary to reinforce the computational efficiency of proposed strategy.

Acknowledgments

This work was supported by National Natural Science Funds for Distinguished Young Scholar under Grants 52025121, National Nature Science Foundation of China under Grants 52172383, 51975118, and 51805081, UCL-ZJU Seed Funds under Grants 2020-21.

Reference

[1] Kham N and New C. Implementation of modern traffic light control system. International journal of scientific and research publications 2014; 4(6): 1-6.

[2] Cao Z, Jiang S, Zhang J, and Guo H. A unified framework for vehicle rerouting and traffic light control to reduce traffic congestion. IEEE transactions on intelligent transportation systems 2016; 8(7): 1958-1973

[3] Zhang J, Tang T, Yan Y, Qu X. Eco-driving control for connected and automated electric vehicles at signalized intersections with wireless charging. Applied Energy 2021; 282: 1-8.

[4] Qu X, Yu Y, Zhou M, Lin C, Wang X. Jointly dampening traffic oscillations and improving energy consumption with electric, connected and automated vehicles: a reinforcement learning based approach. Applied Energy 2020; 257: 1-11

[5] Qin X and Khan A. Control strategies of traffic signal timing transition for emergency vehicle preemption. Transportation research part C: emerging technologies 2012; 25, 1-17.

[6] Koehler L and Kraus J. Simultaneous control of traffic lights and bus departure for priority operation. Transportation Research Part C: Emerging Technologies 2010; 18(3), 288-298.

[7] Zhao Y and Ioannou P. A traffic light signal control system with truck priority. IFAC-PapersOnLine 2016; 49(3), 377-382.

[8] Ma W, Wan L, Yu C, Li Z, Zheng J. Multi-objective optimization of traffic signals based on vehicle trajectory data at isolated intersections. Transportation Research Part C: Emerging Technologies 2020; 120: 1-27.

[9] Liu H, Lu X, Shladover S. Traffic signal control by leveraging cooperative adaptive cruise control (CACC) vehicle platooning capabilities. Transportation Research Part C: Emerging Technologies 2019; 104: 390-407.

[10] Zhuang W, Li S, Zhang X, Kum D, Song Z, Yin G, et al. A survey of powertrain configuration studies on hybrid electric vehicles. Applied Energy 2020; 262, 114553.

[11] He H, Wang C, Jia H, Cui X. An intelligent braking system composed single-pedal and multi-objective optimization neural network braking control strategies for electric vehicle. Applied Energy 2020; 259: 1-14.

[12] Stoicescu A. On fuel–optimal velocity control of a motor vehicle. International Journal of Vehicle Design 1995; 16(2-3), 229-256.

[13] Xu Y, Li H, Liu H, Rodgers M, Guensler R. Eco-driving for transit: an effective strategy to conserve fuel and emissions. Applied Energy 2017; 194: 784-797.

[14] Vahidi A, Sciarretta A. Energy saving potentials of connected and automated vehicles. Transportation Research Part C: Emerging Technologies 2018; 95: 822-843.

[15] Barkenbus J. Eco-driving: an overlooked climate change initiative. Energy policy 2010; 38(2): 762-769.

[16] Asadi B and Vahidi A. Predictive cruise control: utilizing upcoming traffic signal information for improving fuel economy and reducing trip time IEEE Transactions on Control Systems Technology 2010; 19(3): 707–714

[17] NEXTCAR – Next generation energy technologies for connected and automated on-road vehicles. Tech. rep., U.S. Department of Energy.

[18] Li S, Xu S, Huang X, Cheng B, Peng H, Eco-departure of connected vehicles with V2X communication at signalized intersections. IEEE Transactions on Vehicular Technology 2015; 64(12): 5439-5449.

[19] Taiebat M, Stolper S, Xu M. Forecasting the impact of connected and automated vehicles on energy use: a microeconomic study of induced travel and energy rebound. Applied Energy 2019; 247: 297-308.

[20] Katsaros K, Kernchen R, Dianat M, Rieck D, Zinoviou C. Application of vehicular communications for improving the efficiency of traffic in urban areas. Wireless Communications and Mobile Computing 2011; 11: 1657-1667.

[21] Mahler G, Vahidi A. An optimal velocity-planning scheme for vehicle energy efficiency through probabilistic prediction of traffic

signal timing. IEEE Transactions on Intelligent Transportation Systems 2014; 15(6): 2516-2523.

[22] Han X, Ma R, Zhang H. Energy-aware trajectory optimization of CAV platoons through a signalized intersection. Transportation Research Part C: Emerging Technologies 2020; 118, 102652.

[23] Lin Q, Li S, Xu S, Du X, Yang D, Li K. Eco-driving operation of connected vehicle with V2I communication among multiple signalized intersections. IEEE Intelligent Transportation Systems Magazine 2020; 1-13. doi: 10.1109/MITS.2020.3014113.

[24] Mousa S, Ishak S, Mousa R, Codjoe J, Elhenawy M. Deep reinforcement learning agent with varying actions strategy for solving the eco-approach and departure problem at signalized intersections. Transportation research record 2020; 2674(8), 119-131.

[25] Antonio S, Vahidi A. Energy-efficient driving of road vehicles. Springer International Publishing 2020.

[26] Xie L, Luo Y, Zhang D, Chen R, Li K. Intelligent energy-saving control strategy for electric vehicle based on preceding vehicle movement. Mechanical Systems and Signal Processing 2019; 130: 484-501.

[27] Zeng X, Wang J. Globally energy-optimal speed planning for road vehicles on a given route. Transportation Research Part C: Emerging Technologies 2018; 93: 148-160.

[28] He X, Liu X, Liu H. Optimal vehicle speed trajectory on a signalized arterial with consideration of queue. Transportation Research Part C: Emerging Technologies 2015; 61: 106-120.

[29] Guo Q, Angah O, Liu Z, Ban X. Hybrid deep reinforcement learning based eco-driving for low-level connected and automated vehicles along signalized corridors. Transportation Research Part C: Emerging Technologies 2021; 124, 102980.

[30] Wang S and Lin X. Eco-driving control of connected and automated hybrid vehicles in mixed driving scenarios. Applied Energy 2020; 271, 115233.

[31] Alessandrini A, Campagna A, Delle S, Filippi F. Automated vehicles and the rethinking of mobility and cities. Transportation Research Procedia 2015; 5: 145-160.

[32] Shao Y, Sun Z. Eco-approach with traffic prediction and experimental validation for connected and autonomous vehicles. IEEE Transactions on Intelligent Transportation Systems 2020; 1-11. doi: 10.1109/TITS.2020.2972198.

[33] Sun C, Guanetti J, Borrelli F, Moura S. Optimal eco-driving control of connected and autonomous vehicles through signalized intersections. IEEE Internet of Things Journal 2020; 7(5): 3759-3773.

[34] Bakibillah A, Kamal M, Tan C, Hayakawa T, Imura I. Event-driven stochastic eco-driving strategy at signalized intersections from self-driving data. IEEE Transactions on Vehicular Technology 2019; 68(9): 8557-8569.

[35] Yang H, Rakha H, Ala M. Eco-cooperative adaptive cruise control at signalized intersections considering queue effects. IEEE Transactions on Intelligent Transportation Systems 2016; 18 (6): 1575-1585.

[36] Yong J, Ramachandaramurthy V, Tan K, Mithulananthan N. A review on the state-of-the-art technologies of electric vehicle, its impacts and prospects. Renewable and Sustainable Energy Reviews 2015; 49: 365-385.

[37] Pedrosa D, Monteiro V, Goncalves H, Martins J, Afonso J. A case study on the conversion of an internal combustion engine vehicle into an electric vehicle. 2014 IEEE Vehicle Power and Propulsion Conference (VPPC). 2014: 1-5.

[38] Howey D, Martinez-Botas R, Cussons, Lytton L. Comparative measurements of the energy consumption of 51 electric, hybrid and internal combustion engine vehicles. Transportation Research Part D: Transport and Environment 2011; 16(6): 459-464.

[39] Sweeting W, Hutchinson A, Savage S. Factors affecting electric vehicle energy consumption. International Journal of Sustainable Engineering 2011; 4(3): 192-201.

[40] Gao J, Chen H, Li Y, Chen J, Zhang Y, Dave K, et al. Fuel consumption and exhaust emissions of diesel vehicles in worldwide harmonized light vehicles test cycles and their sensitivities to eco-driving factors. Energy Conversion and Management 2019; 196: 605-613.

[41] Desreveaux A, Bouscayrol A, Trigui R, Castex E, Klein J. Impact of the velocity profile on energy consumption of electric vehicles. IEEE Transactions on Vehicular Technology 2019; 68(12): 11420-11426.

[42] Han J, Vahidi A, Sciarretta A. Fundamentals of energy efficient driving for combustion engine and electric vehicles: an optimal control perspective. Automatica 2019; 103: 558-572.

[43] Gao Z, LaClair T, Ou S, Huff S, Wu G, Hao P, et al. Evaluation of electric vehicle component performance over eco-driving cycles. Energy 2019; 172: 823-839.

[44] Rajamani R. Vehicle dynamics and control. Springer Science & Business Media 2011.

[45] Biral F, Da Lio M, and Bertolazzi e. Combining safety margins and user preferences into a driving criterion for optimal control-based computation of reference maneuvers for an ADAS of the next generation. IEEE Intelligent Vehicles Symposium, Las Vegas, NV, USA, 2005: 36-41.

[46] Larminie J and Lowry J. Electric vehicle technology explained. John Wiley & Sons 2012.

[47] Srivastava N and Haque I. A review on belt and chain continuously variable transmissions (CVT): dynamics and control. Mechanism and Machine Theory 2009; 44(1):19-41.

[48] Zhuang W, Zhang X, Li D, Wang L, Yin G. Mode shift map design and integrated energy management control of a multi-mode hybrid electric vehicle. Applied Energy 2017; 204: 476-488.

[49] Polson N, Sokolov V. Deep learning for short-term traffic flow prediction. Transportation Research Part C: Emerging Technologies 2017; 79: 1-17.

[50] Treiber M, Hennecke A, Helbing D. Congested traffic states in empirical observations and microscopic simulations. Physical Review E 2000; 62(2): 1805-1824.

[51] Bellman R. Dynamic programming. Science 1996; 153(3731): 34-37.

[52] Zhu C, Lu F, Zhang H, Sun J, Mi C. A real-time battery thermal management strategy for connected and automated hybrid electric vehicles (CAHEVs) based on iterative dynamic programming. IEEE Transactions on Vehicular Technology 2018; 67(9): 8077-8084.

[53] Kesting A, Treiber M, Schönhof M, Helbing D. Extending adaptive cruise control to adaptive driving strategies. Transportation Research Record 2007; 2000(1): 16-24.

[54] Shladover S, Su D, Lu X. Impacts of cooperative adaptive cruise control on freeway traffic flow. Transportation Research Record 2012; 2324(1): 63-70.

[55] Zhang W, Qu L, Xu S, Li B, Chen C, Yin G. Integrated energy-oriented cruising control of electric vehicle on highway with varying slopes considering battery aging. Science China Technological Sciences 2019; 63(1): 155-165.

[56] Li S, Peng H. Strategies to minimize the fuel consumption of passenger cars during car-following scenarios. Proceedings of the Institution of Mechanical Engineers, Part D: Journal of Automobile Engineering 2012; 226(3): 419-429.

[57] Lin Q, Li S, Du X, Zhang X, Peng H, Luo Y, et al. Minimize the fuel consumption of connected vehicles between two red-signalized intersections in urban traffic. IEEE Transactions on Vehicular Technology 2018; 67(10): 9060-9072.